Electronic Supplementary Information (ESI) for Soft Matter

Understanding Creep Suppression Mechanism in Polymer Nanocomposites through Machine Learning

Entao Yang,[a] James F. Pressly,[b] Bharath Natarajan,[c] Robert Colby,[c] Karen I. Winey,*[b] and Robert A. Riggleman*[a]

ESI includes:
Figures S1 - S15
Tables S1 - S3
ESI text
ESI Reference

1 Details of systems examined

1.1 Simulation systems

Table S 1 Simulation System Conditions. Loadings (ϕ_{NP}), NP nominal radius (r), and Polymer-NP interactions (ε_{PN})

System	ϕ_{NP} ($vol\%$)	r (σ)	ε_{PN}	T_g	number of NPs	Average T_{crit} (τ_{LJ})
1	5	3	2.0 (strong)	0.47	20	39459
2	10	3	0.5 (weak)	0.47	42	43641
3	10	5	0.5 (weak)	0.46	9	32426
4	10	3	1.0 (neutral)	0.47	42	61154
5	10	5	1.0 (neutral)	0.47	9	42884
6	10	3	2.0 (strong)	0.48	42	152011
7	10	5	2.0 (strong)	0.47	9	77355
8	15	3	2.0 (strong)	0.49	68	331159
9	15	5	2.0 (strong)	0.47	14	129521
10	20	3	2.0 (strong)	0.50	96	1260857
11	20	5	2.0 (strong)	0.48	20	398619
12		neat polymer		0.46	0	22594

1.2 Experimental systems

Table S 2 Experimental System Details. Nanoparticle Diameters (d_{NP}), Loadings (ϕ_{NP}), and T_g for Nanocomposites and Neat P2VP.

d_{NP} (nm)	ϕ_{NP} ($vol\%$)	T_g ($^\circ C$)
13.0	5.3	104.2
	10.3	104.9
	16.2	104.9
	21.2	105.1
52.0	4.3	104.2
	8.9	103.8
	13.6	103.8
	18.4	104.0
neat P2VP		104.0

* Corresponding authors
[a] Department of Chemical & Biomolecular Engineering, University of Pennsylvania, Philadelphia, PA 19104, USA. E-mail: rrig@seas.upenn.edu
[b] Department of Materials Science & Engineering, University of Pennsylvania, Philadelphia, PA 19104, USA. E-mail: winey@seas.upenn.edu
[c] ExxonMobil Technology and Engineering Company, Annandale, NJ 08801, USA

2 Symbols and parameters used

Table S 3 Symbols and Parameters

Symbols and parameters	Definition
S	softness
$P_R(S)$	particles' probability of rearrangements at a given S
$P_{R,avg}(S)$	bulk-average $P_R(S)$
Σ	entropic barrier
Σ_1	slope of Σ-S curve
Σ_0	intercept of Σ-S curve
ΔE	energy barrier
e_1	slope of ΔE-S curve
e_0	intercept of ΔE-S curve
P_D (P_D^*)	structure-dependent process
P_I (P_I^*)	structure-independent process
F_D	free energy barrier of the structure-dependent process
F_I	free energy barrier of the structure-independent process
P_{np}	ratio of $P_R(S)$ over $P_{R,avg}(S)$ at different positions
a_1	slope of $ln(P_{np})$-S curve
a_0	intercept of $ln(P_{np})$-S curve
R_{acc}	accumulated rearrangement numbers
ε	true strain
k_1	slope of $\varepsilon - R_{acc}$ (normalized) curve
k_0	intercept of $\varepsilon - R_{acc}$ (normalized) curve

3 Nanoparticle dispersion state: large nanoparticles, neutral interaction, and weak interaction

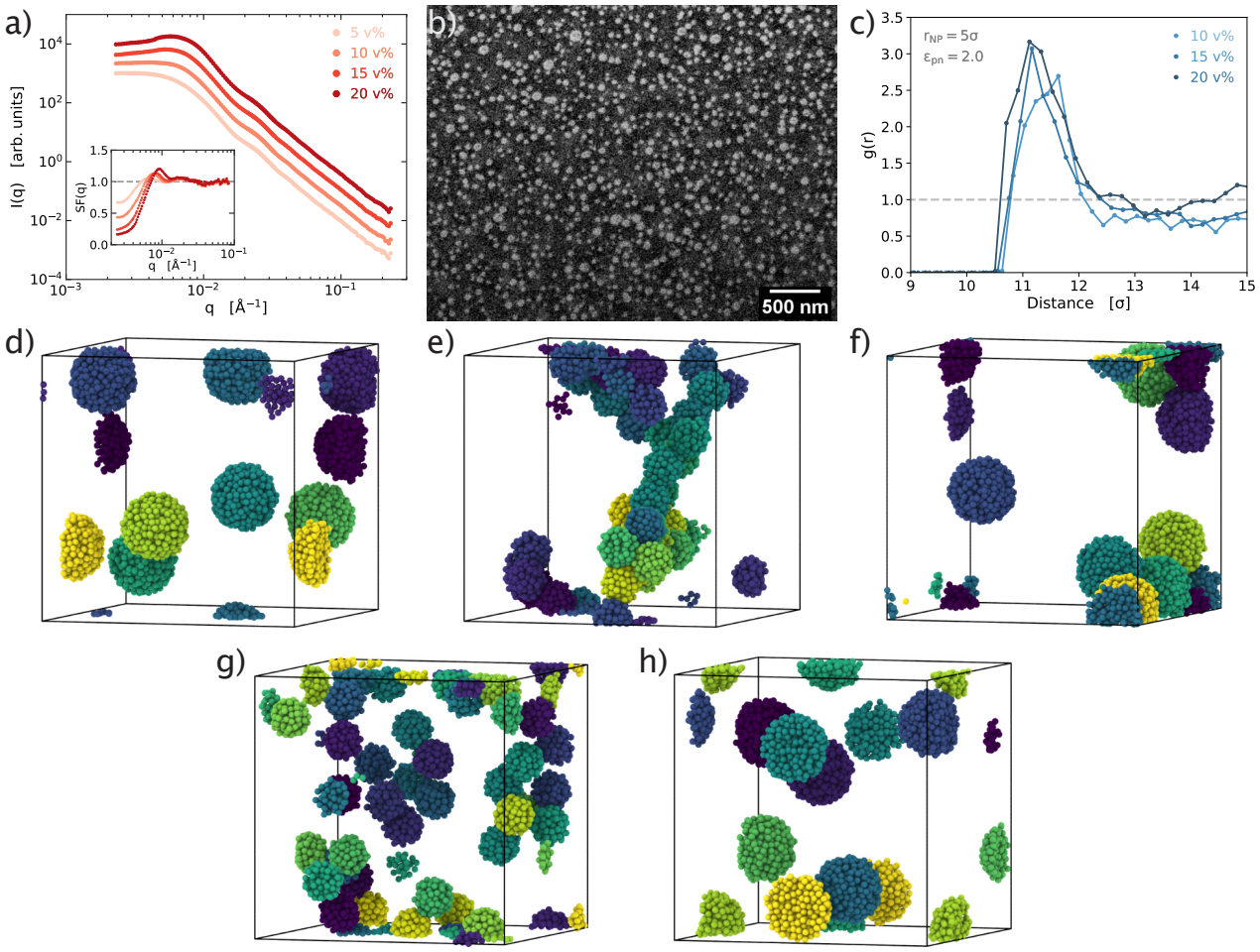

Fig. S 1 SAXS measurements of (a) NP52 nanoparticle composites showing excellent nanoparticle dispersion. Insets in (a) show the nanoparticle structure factor. Representative SEM image of the 15 *vol%* NP52 PNC is shown in (b). Pair distribution functions for nanoparticles in the (c) large particle composites simulations showing good dispersion. Visualization of the nanoparticle distributions are shown in (d) large strong interaction, (e) small weak interaction, (f) large weak interaction, (g) small neutral interaction, and (h) large neutral interaction particle composites. These results suggest that neutral interaction nanoparticles are well dispersed but weak interaction nanoparticles aggregate in the composites.

4 Dynamical decomposition in different systems and T

In addition to the 10 *vol%* loading PNCs with small and neutral polymer-NP interaction NPs described in the main text, we also applied our dynamical decomposition model to two other systems: small NPs with strong polymer-NP interactions and large NPs with neutral polymer-NP interactions. (see Figure S2a - 2d) We also plot the newly introduced quantity, P_{np} (the ratio of $P_R(S)$ over $P_{R,ave}(S)$), as a function of softness for several temperatures, demonstrating that the exponential relation between P_{np} and softness is invariant to temperature within the range tested. Results are presented in Figure S2e - 2g.

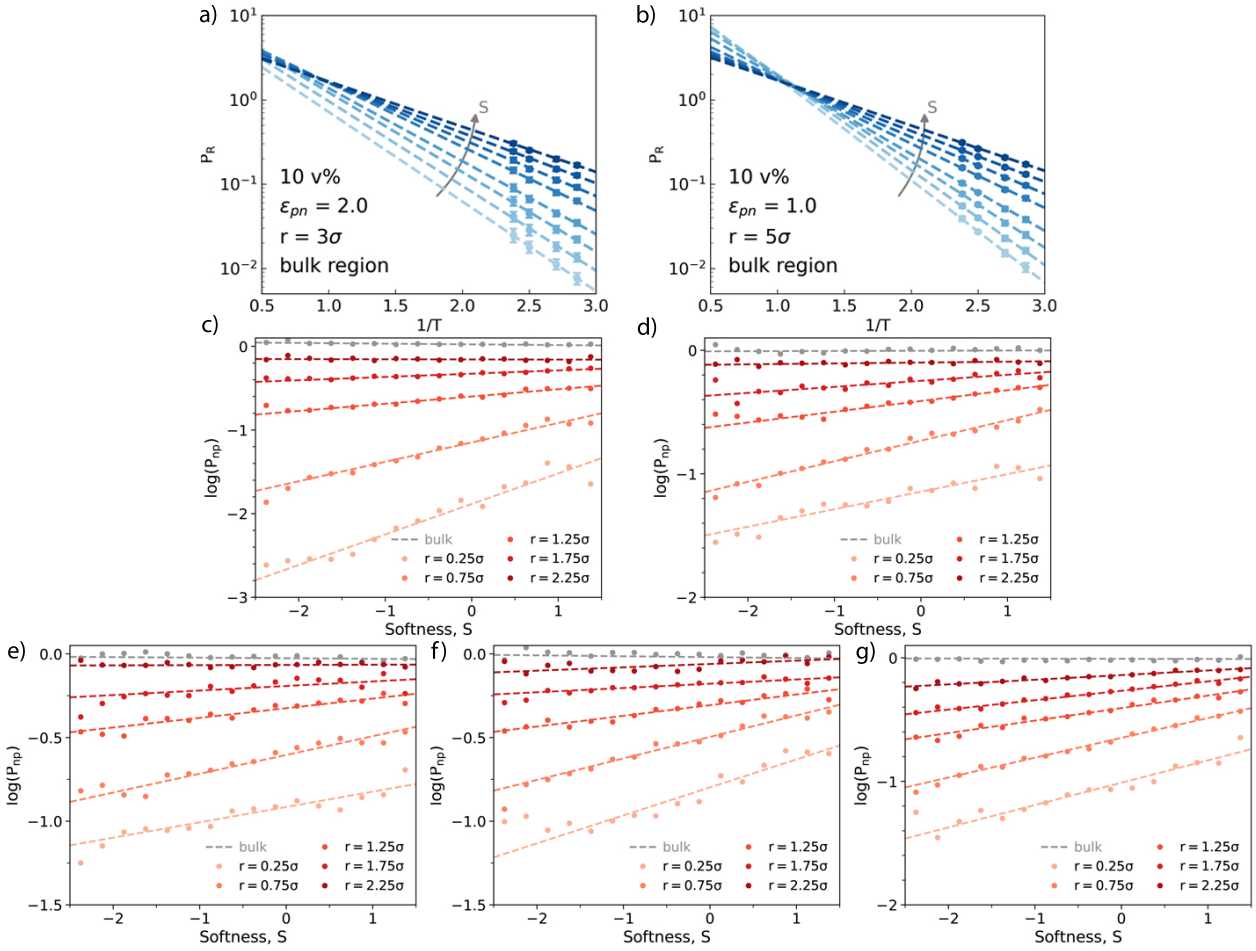

Fig. S 2 $P_R(S)$, as a function of $1/T$ for softness values ranging from $S=-2.75$ (light blue) to $S=1.25$ (dark blue): (a) 10 *vol%* PNCs with small and strong interaction NPs; (b) 10 *vol%* PNCs with large and neutral interaction NPs. (c-g) P_{np} as a function of S for five positions and the bulk-average dynamics in 10 *vol%* PNCs: (c) $r=3\sigma$, $\varepsilon_{pn}=2.0$, $T=0.40$; (d) $r=5\sigma$, $\varepsilon_{pn}=1.0$, $T=0.40$; (e) $r=3\sigma$, $\varepsilon_{pn}=1.0$, $T=0.35$; (f) $r=3\sigma$, $\varepsilon_{pn}=1.0$, $T=0.37$; (g) $r=3\sigma$, $\varepsilon_{pn}=1.0$, $T=0.42$.

5 Regular dynamical decomposition fails near NPs

When we following the protocol described in the main text and use Equation 1 to describe dynamics near the polymer-NP interface, we observe a breakdown in the relationship between the $P_R(S)$ and S. As shown in Figure S3a and S3b, the left-extended fitting curves of P_R versus $1/T$ at different softness values do not have a shared intersection. Because of this, ΔE and Σ do not follow a linear relationship with softness near the polymer-NP interface, unlike the bulk-average dynamics (Figure 3d in the main text). This can be seen in Figure S3c and S3d.

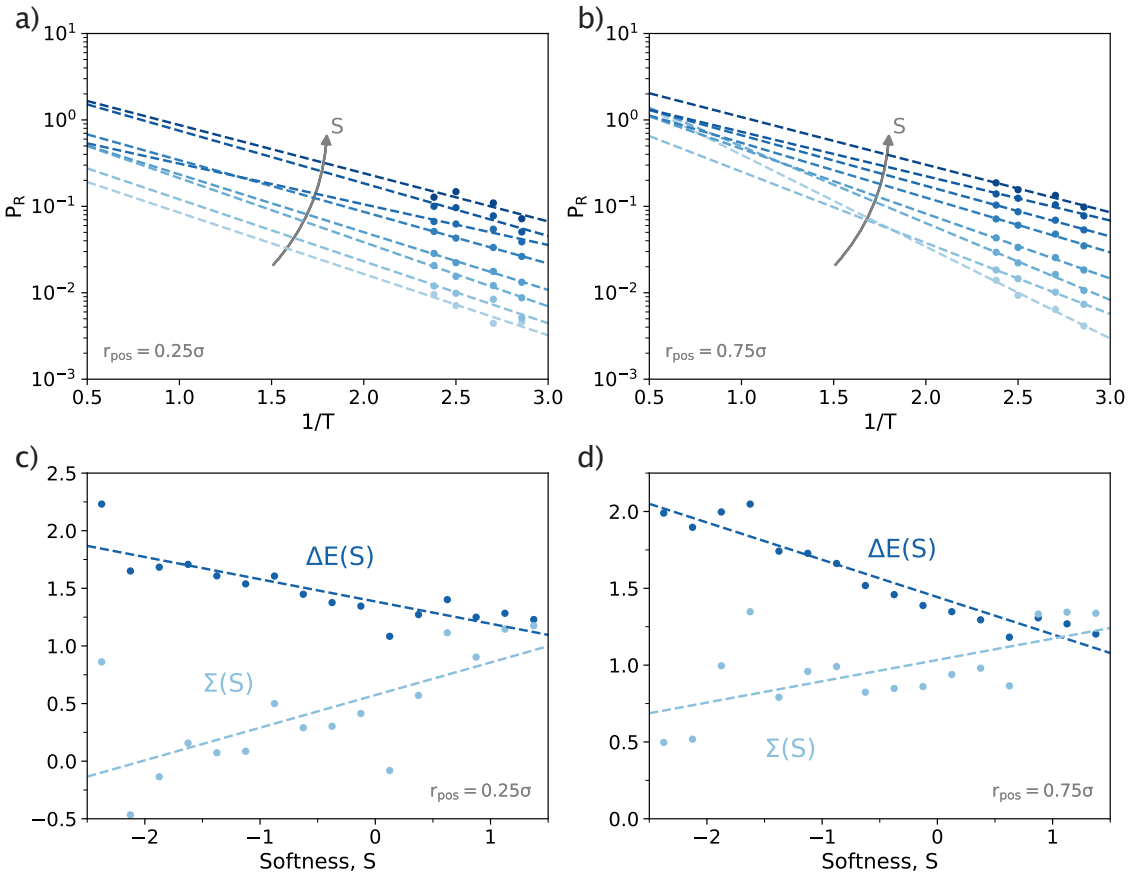

Fig. S 3 $P_R(S)$, as a function of $1/T$ for softness values ranging from $S = -2.75$ (light blue) to $S = 1.25$ (dark blue) at (a) $r_{pos} = 0.25\sigma$ and (b) $r_{pos} = 0.75\sigma$. ΔE and Σ as a function of softness near NPs at (c) $r_{pos} = 0.25\sigma$ and (d) $r_{pos} = 0.75\sigma$. Results are obtained through regular dynamical decomposition (Equation 1 in the main text).

6 Average softness and softness distributions at different positions

The presence of NPs can alter the nearby polymer packing, thus we expect to see a modified softness distribution near the NP surface. In Figure S4a, we plot softness as a function of r_{pos} for 10 $vol\%$ PNCs, with strong and neutral polymer-NP interactions at $T = 0.40$. As expected, softness is reduced near the NP surface, with stronger polymer-NP interactions causing a greater decrease. The deviation from bulk-average softness for $r_{pos} < 1.75\sigma$ matches the change in P_D^* observed in Figure 4a in the main text, because softness is a significant component of the structure dependent process in rearrangements. Previous work has reported that softness follows a normal distribution in bulk systems,[1] and here we find that this behavior holds true in PNCs as well. As shown in Figure S4b, softness at different distances from the polymer-NP interface follows a normal distribution, with the center of the distribution shifting as the average softness varies.

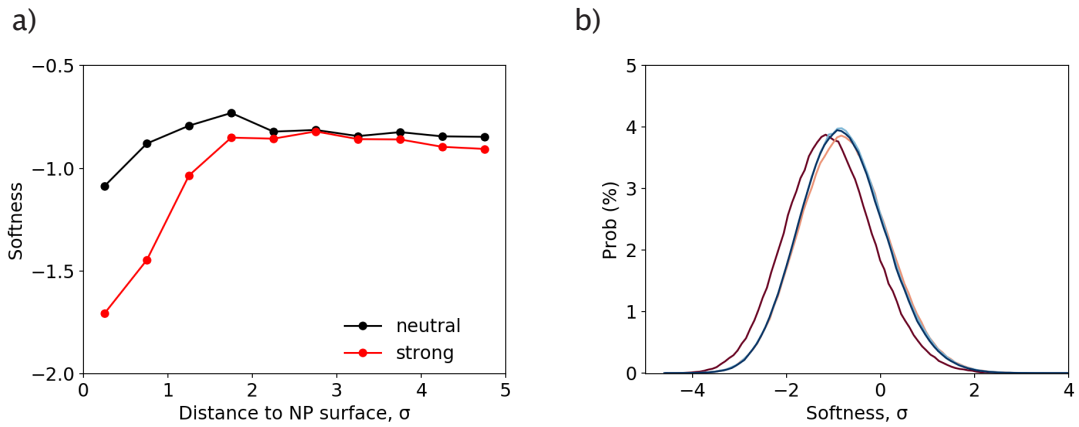

Fig. S 4 (a) Average softness as a function of distance to NP surface in 10 $vol\%$ PNCs, for both strong interaction and neutral interaction NPs. (b) softness distribution at different positions in the neutral interaction PNCs. Color gradient represents different positions: $r_{pos} = 0.25$ (dark red), 1.25 (light red), 2.75 (light blue), and 3.75 σ (dark blue). Results are measured at $T = 0.40$.

7 Strain-time curves of neutral interaction and strong interaction PNCs

To further expand our decomposition model from undeformed composites to composites within the constant-strain-rate creep regime, the limit of linear response (versus time) under different stresses must be determined. Strain-time curves depicting composite deformation under eight different stresses ($\sigma_c = 0.3$ to 0.9) are presented in Figure S5. For both strong and neutral polymer-NP interaction systems, stresses at or below 0.6 (all the red curves) exhibit a constant-strain-rate response.

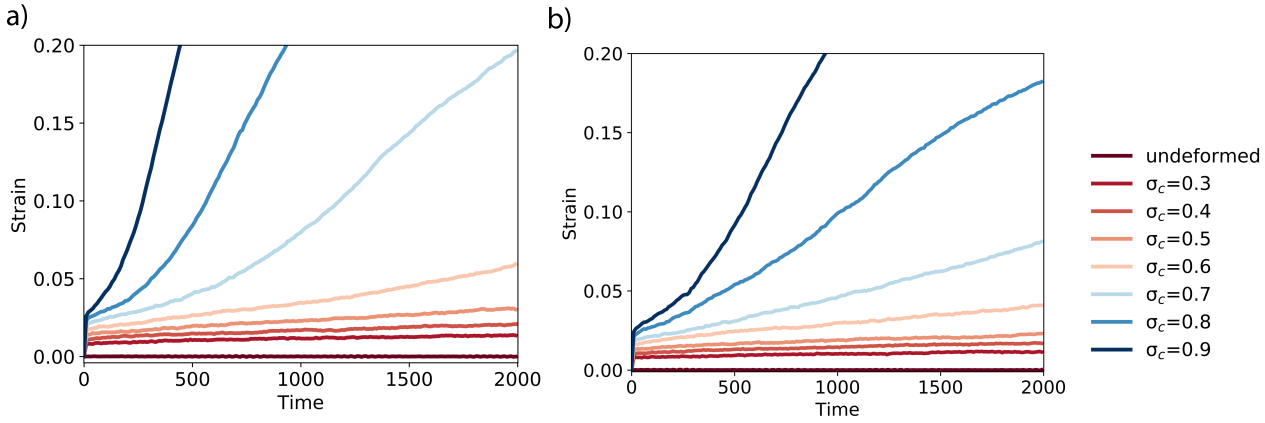

Fig. S 5 Strain-time response curves for 10 $vol\%$ PNCs with (a) neutral and (b) strong polymer-NP interactions for 8 different stresses ($\sigma_c = 0$ and $\sigma_c = 0.3$ to 0.9). Color gradient represents the stress gradient, from undeformed PNCs (dark red) to $\sigma_c = 0.9$ (dark blue).

8 Softness change during creep

Because the softness values are used to determine the structure-dependent process of rearrangement in our dynamical decomposition, it is necessary to monitor the change in softness during creep deformation. Figure S6a shows the average softness of PNCs as a function of deformation time. For applied stresses that result in a constant-strain-rate response ($\sigma_c \leq 0.6$, red curves), average softness is almost constant after the initial elastic response. For greater applied stresses, there are significant changes in average softness as deformation progresses (blue curves). These results are consistent with previous work in a wide range of amorphous materials, where the shift in average softness before yielding is one order smaller than the standard deviation of softness distribution.[2] Figure S6b and S6c show the softness profiles near the polymer-NP interface under different applied stresses for the entire deformation process ($t \leq 2000$) and the constant-strain-rate region (linear response versus time) respectively ($t \leq 1000$ for $\sigma_c = 0.7$, $t \leq 500$ for $\sigma_c = 0.8$, and $t \leq 250$ for $\sigma_c = 0.9$). In other words, only the blue curves are different in Figure S6b and S6c. These suggest that change in softness spatial distribution is small within the constant-strain-rate creep regime, which can also be proven by Figure S6d.

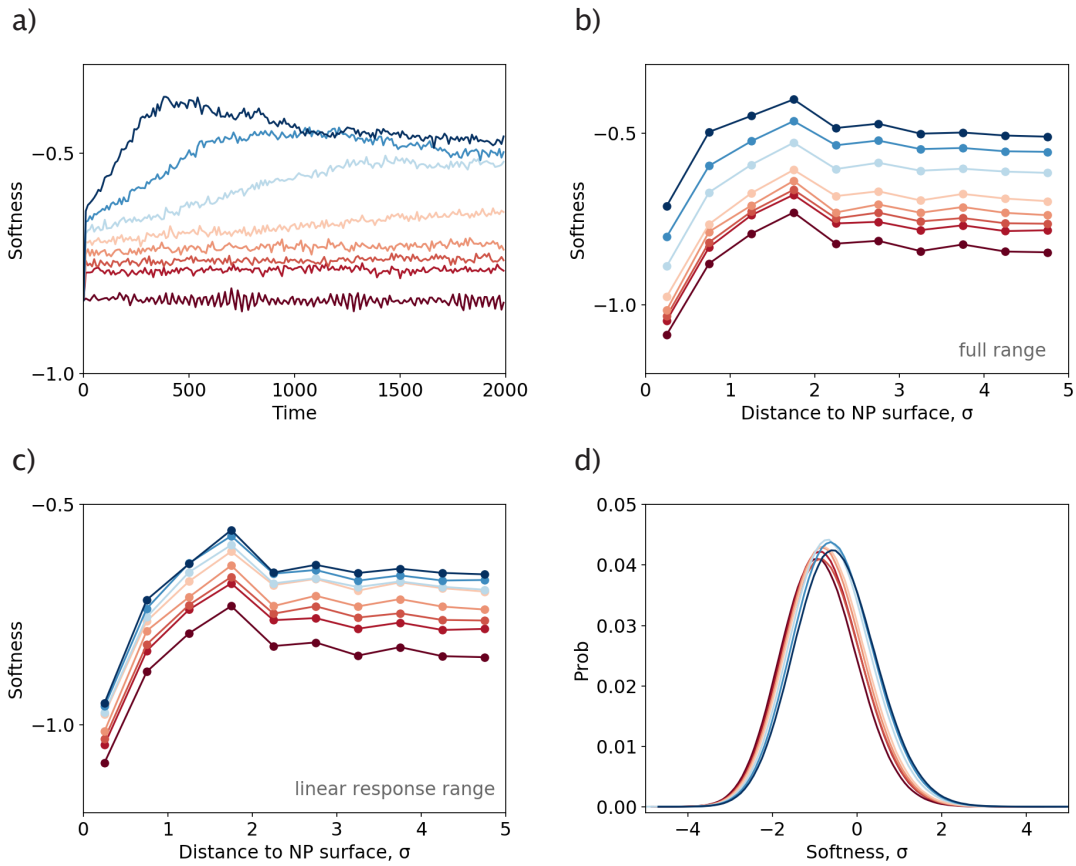

Fig. S 6 Softness change during creep deformation for neutral interaction PNCs at $T = 0.40$. (a) Average softness of the system as a function of time. (b) Softness as a function of r_{pos} for the full deformation regime. (c) Softness as a function of r_{pos} for the constant-strain-rate regime, determined in 5a. (d) Softness distribution in PNCs under different stresses. The color gradient represents the same stress gradient in 5, from $\sigma_c = 0$ (dark red) to $\sigma_c = 0.9$ (dark blue).

9 Change in $P_R(S)$ during creep

In Figure S7, we plot $P_R(S)$ as a function of both stress, σ_c, and position, r_{pos}, where the color gradient represents the magnitude of $P_R(S)$. Here, for the ease of visualization, we pick $S = 0.375$, results at other softness values are qualitatively same.

We observe that the change in $P_R(S)$ with σ_c is much smaller than the change in $P_R(S)$ with r_{pos}, especially within the constant-strain-rate creep region. This $P_R(S) - S$ relation together with the softness distribution in Figure S6 suggests that our dynamical decomposition model should remain valid within the constant-strain-rate regime.

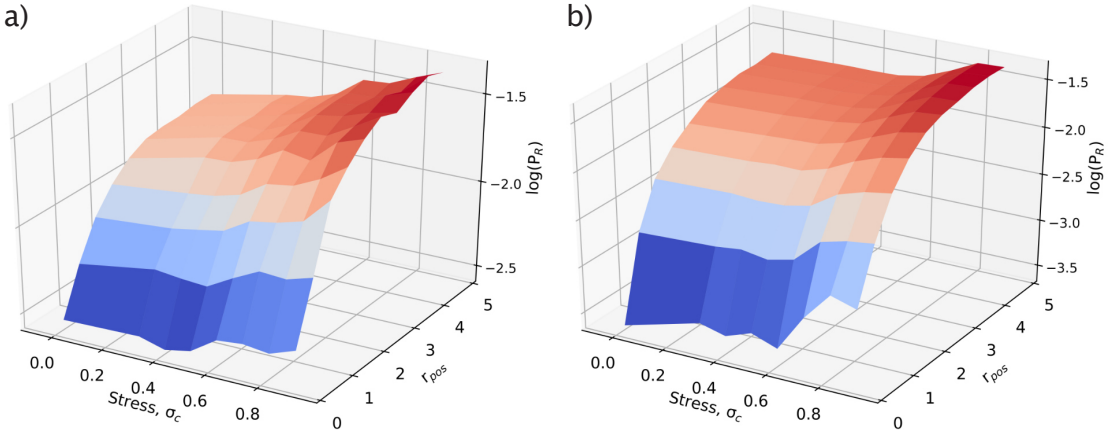

Fig. S 7 $P_R(S)$ as a function of stress, σ_c, and position, r_{pos}, in 10 $vol\%$ PNCs, containing small NPs with (a) neutral and (b) strong polymer-NP interactions.

10 Dynamical decomposition for the bulk-average dynamics of PNCs under creep

Because the change in softness and change in $P_R(S)$ is small within the constant-strain-rate regime, it is reasonable to speculate that our dynamical decomposition model should still work within this regime. Here, we follow the dynamical decomposition protocol outlined in the main text and plot the bulk-average $P_R(S)$ as a function of $1/T$ for four different stresses, in Figure S8. As expected, $P_R(S)$ follows Arrhenius behavior at each softness and the left-extended fitting curves share a same intersection point (indicating that ΔE and Σ decays linearly with softness). Thus, for the bulk-average dynamics in PNCs under constant-strain-rate creep deformation, Equation 1 still holds.

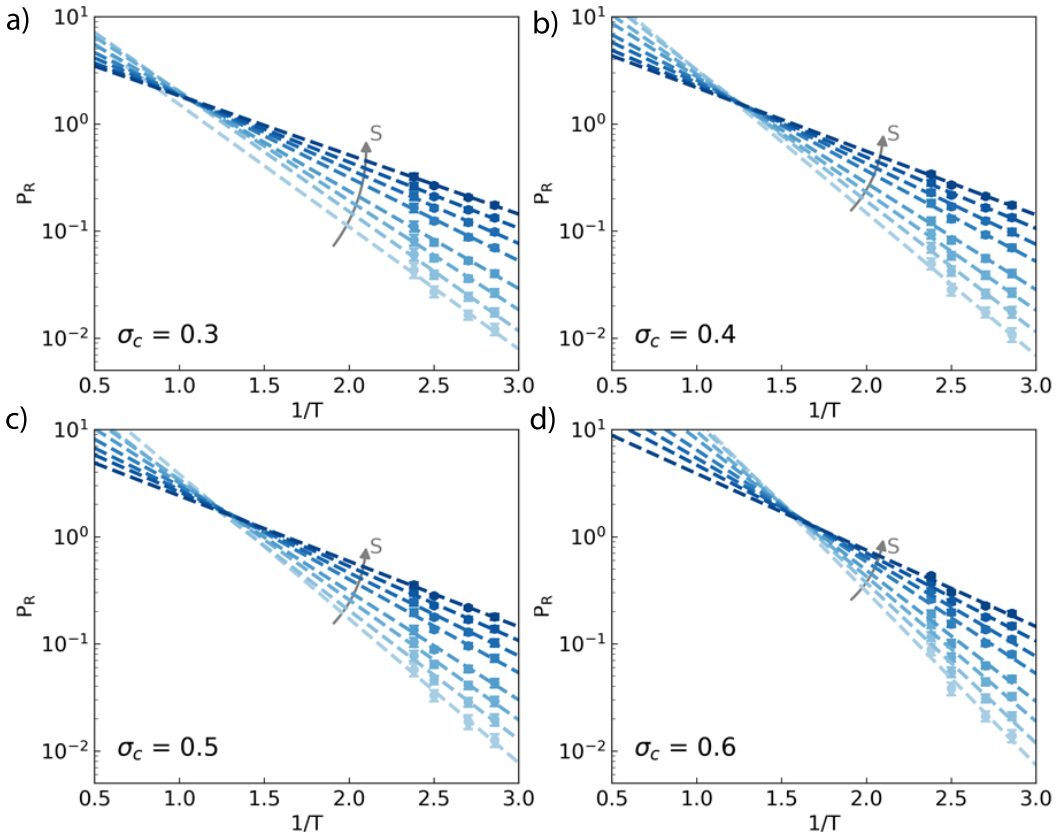

Fig. S 8 Bulk-average $P_R(S)$ as a function of $1/T$ for softness values ranging from $S = -2.75$ (light blue) to $S = 1.25$ (dark blue): (a) $\sigma_c = 0.3$; (b) $\sigma_c = 0.4$; (c) $\sigma_c = 0.5$; (d) $\sigma_c = 0.6$.

11 P_{np} as a function of softness under creep, for different positions and stresses

In Figure S9 we plot P_{np} as a function of softness for different positions near the polymer-NP interface while under an constant applied stress. Results show that the exponential relation between P_{np} and S remains valid under constant-strain-rate creep deformation. Therefore, our dynamical decomposition model can be safely expanded to systems undergoing constant-strain-rate creep deformation and the effect of the applied stress can be described by the six parameters in our model $(\Sigma_i, \Delta E_i, a_i)$.

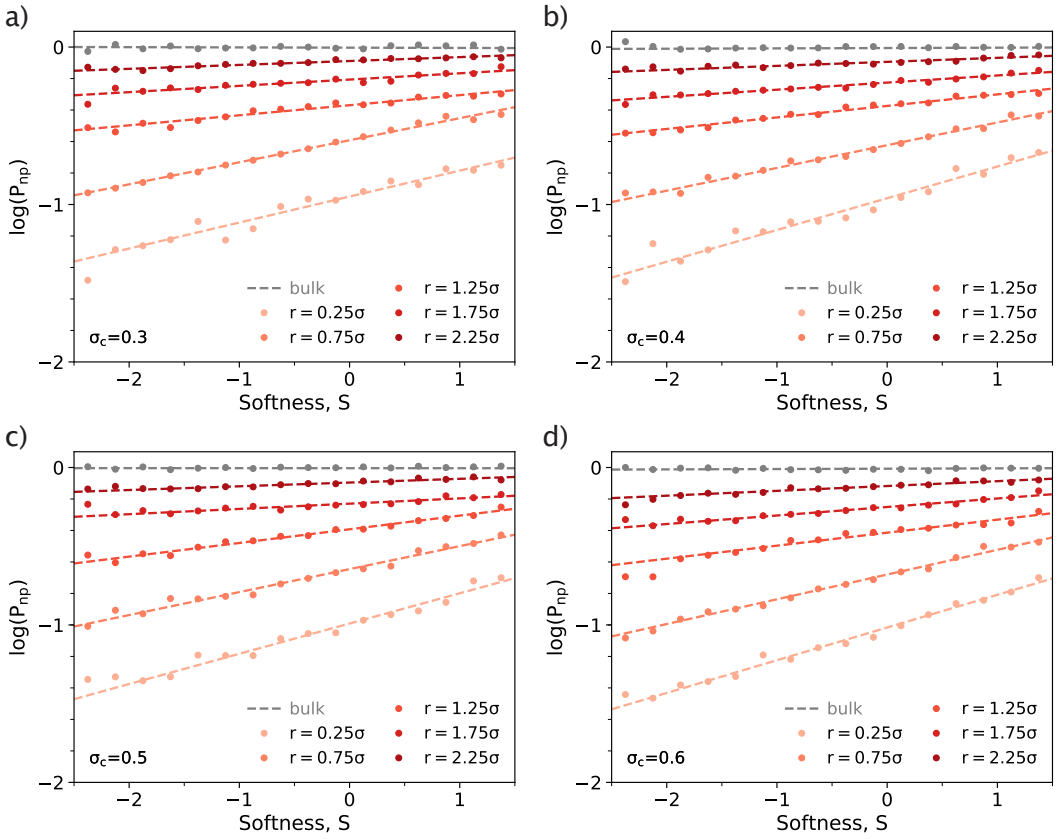

Fig. S 9 P_{np} as a function of softness for five positions ($r_{pos} = 0.25$ to 2.25σ) and the bulk region, at $T = 0.40$: (a) $\sigma_c = 0.3$; (b) $\sigma_c = 0.4$; (c) $\sigma_c = 0.5$; (d) $\sigma_c = 0.6$. Different colors represents the different positions (r_{pos}).

12 Particle rearrangement ratio as a function of time under creep

To connect the microscopic dynamical picture to the macroscopic mechanical response, we focus on the relationship between strain and the normalized accumulated rearrangement number, $\overline{R_{acc}}$. Results in Figure S10 indicate that the particle rearrangement ratio (number of rearranging monomers normalized by the total number of monomers), in each frame, is quite stable within the constant-strain-rate creep regime. This suggests that the total number of particle rearrangements, and therefore $\overline{R_{acc}}$, will increase linearly with time under constant-strain-rate creep deformation. Because strain increases linearly with time in this regime as well, we can predict the system's strain response from $\overline{R_{acc}}$ using Equation 4.

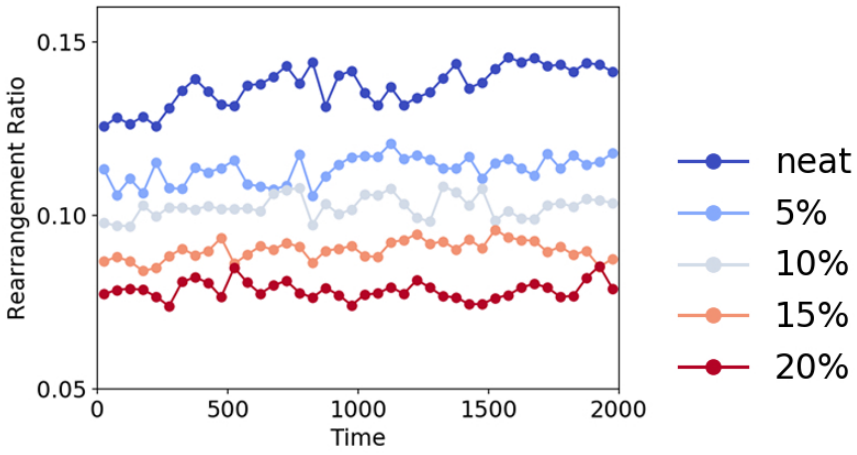

Fig. S 10 Particle rearrangement ratio ($R_{num}/N_{polymer}$) as a function of time for different composites, at $T = 0.40$.

13 Predict strain from initial softness distribution

As we have already connected the strain to the accumulated rearrangement number, $\overline{R_{acc}}$, predicting $\overline{R_{acc}}$ from softness will enable us to predict strain response directly from the structure information. This can be achieved through the previously proposed dynamical decomposition model. According to definition of $P_R(S)$, we have:

$$\overline{R_{acc}} = \frac{1}{N_t}\int_0^{time}\int_0^{\infty}\int_{S_0}^{S_\infty} NP_R\, dSdr_{pos}dt \simeq t\cdot\left(P_I\sum_{S_{min}}^{S_{max}} N_s^{bulk}P_D + \sum_{r_{pos}=0.25}^{4.75} P_I^*\sum_{S_{min}}^{S_{max}} N_sP_D^*\right) \tag{1}$$

Here, N_t is the total number of polymer particles in the composites, N is the number of particles (at certain softness and position). S_{min} and S_{max} are the minimum and maximum softness. N_s^{bulk} is the number of particles (at certain softness and position) in the bulk region and N_s is that in the near-NP region. We choose $r_{pos} = 4.75\sigma$ as the cutoff point for near-NP region, which fully captures the deviations of the structure-dependent and independent components of monomer rearrangement from the bulk-average value, in Figures 4 and 5. Using the result of Equation 1 we can then predict the strain response of the PNC using Equation 4 in the main text.

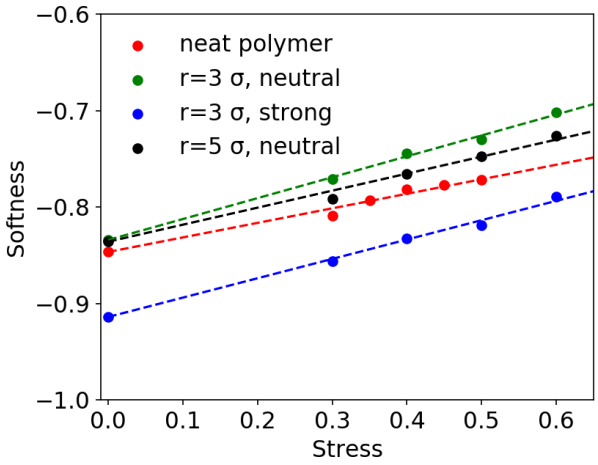

Fig. S 11 Mean softness change due to elastic response as a function of stress at $T = 0.40$.

Theoretically, softness distribution in Equation 1 is collecting from the entire deformation process and is time dependent. Thus, the last step is predicting the softness distribution during creep from the initial structure. As shown in Figure S6, mean softness is quite stable after the initial elastic response and the width of the softness distribution is also unchanged. This suggests that the prediction can be reframed as the prediction from initial mean softness to that right after the elastic response. In Figure S11, we plot the mean softness after the elastic response as a function of stress at $T = 0.40$ and find that it grows linearly with stress.

This agrees with the finding that softness has a universal constant response to strain for disordered materials and the elastic strain response is proportional to stress.[2] These together prove that:

$$S_{elastic} = w_1\sigma_c + S_{\sigma_c=0} \tag{2}$$

where ($S_{elastic}$) is the mean softness after elastic response and ($S_{\sigma_c=0}$) is the mean softness of the undeformed PNCs.

In Figure S12, we plot the flow chart of the prediction process. $f_2(R_{acc})$, $P_R(S, r_{pos})$ and $f_1(\sigma_c)$ are corresponding to Equation 4, Equation 3 and Equation 2 respectively. In this prediction, we have nine parameters, where Σ_0, Σ_1, e_0, e_1, k_0, k_1, and w_1 are functions of stress and T, and a_0 and a_1 are functions of stress, T, and r_{pos}. The only input information is the softness distribution at different positions measured in the pre-deformation PNCs.

Besides the prediction in different systems shown in the main text (Figure 6b), here we also tested it for different systems at several different temperatures. Results are shown in Figure S13 and in good agreement with the measured strain values.

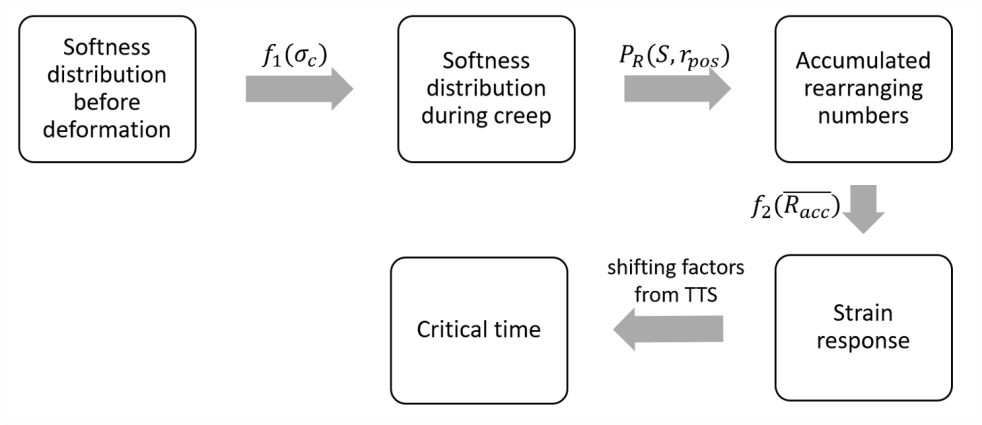

Fig. S 12 Flow chart of the prediction protocol: from the initial softness distribution of undeformed PNCs to the critical time

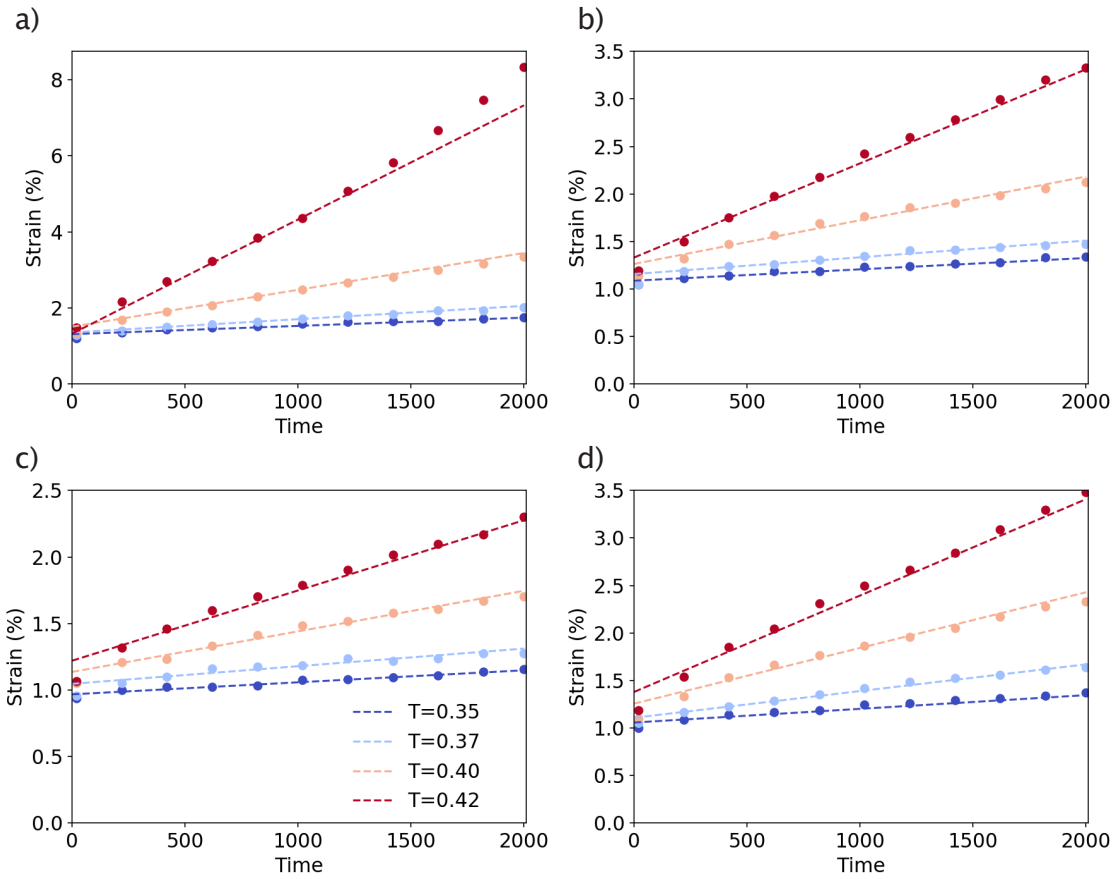

Fig. S 13 Predicting strain from softness at different temperatures for (a) neat polymer, (b) 10 *vol%* loading with small NPs and neutral polymer-NP interactions, (c) 10 *vol%* loading with small NPs and strong polymer-NP interactions, and (d) 10 *vol%* loading with large NPs and neutral polymer-NP interactions.

14 Numerical justification of treating NP sites as polymer sites

In previous work, we have shown that treating nanoparticle sites as polymer sites does not qualitatively affect softness analysis in a polymer nanopillar with one NP, embedded in the center of pillar, by comparing results with varied cut-off distances.[3] Here, we take a similar method and use structure functions with $R_{cutoff} = 1.5$ and 3.5σ to calculate softness in 10 *vol%* PNCs. Varying cutoff distance changes the number of NP sites included in the softness analysis. Therefore, a significant change in softness for different cutoff values would invalidate our approximation. In Figure S14, we plot $P_R(S)$ as a function of softness and distance to NP surface respectively. The qualitatively similar results at each cutoff distance

indicate that our approximation is still valid in PNCs containing multiple nanoparticles.

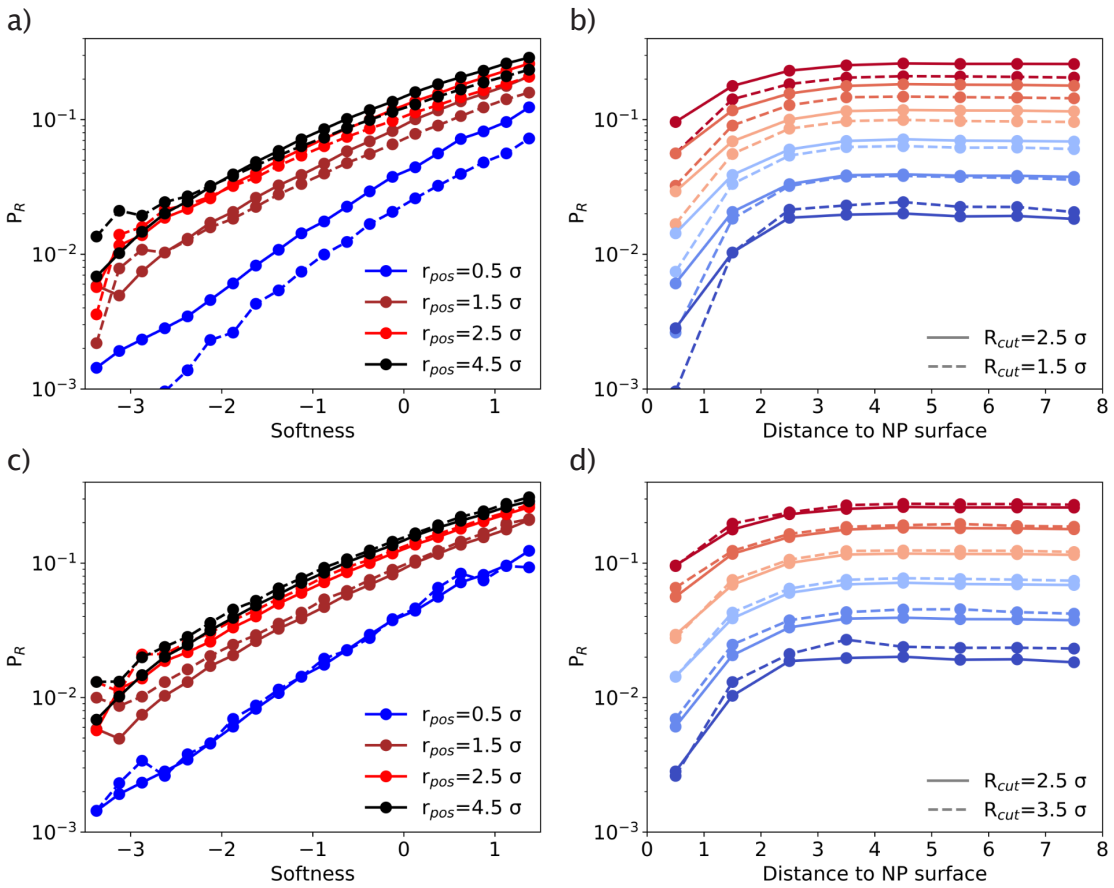

Fig. S 14 Varying cutoff distance of structure functions in 10 *vol%* PNCs with small, strong interaction NPs: (a) $P_R(S)$ as a function of S, $R_{cutoff} = 1.5\sigma$; (b) $P_R(S)$ as a function of r_{pos}, $R_{cutoff} = 1.5\sigma$; (c) $P_R(S)$ as a function of S, $R_{cutoff} = 3.5\sigma$; (d) $P_R(S)$ as a function of r_{pos}, $R_{cutoff} = 3.5\sigma$.

We now need to know whether the deviation from regular dynamical decomposition near the polymer-NP interface is due to this approximation or not. To answer this question, we draw insights from the idea of TrAdaBoost algorithm[4], which is a representative algorithm of transfer learning.

The basic idea of transfer learning is storing knowledge learned while solving one problem and applying it to a different but related problem. The TrAdaBoost algorithm is proposed to get rid of a fundamental assumption of traditional machine learning, that the training set and the test set have the same distribution, which is not always true in practice. In TrAdaBoost, a training set consists of samples from two distributions, one is the same as the test set, T_s, and the other is not, T_d. During training, the weight of samples from T_s are increased when they are mislabeled. The weights of samples from T_d, in contrast, are increased when they are correctly labeled. Using this algorithm we make the most use of samples from T_s and also find similar samples (compared with test set) from T_d. More details about this algorithm can be found in reference[4].

In this study, as shown in Figure S4, the softness distribution is different near the NP surface, as compared with the bulk region. In other words, the training dataset (neat polymer system) and the test data set (PNCs system) have different distributions. Thus, we divided polymers in our PNCs into two groups, polymer monomers near NPs ($r_{pos} < 2.5\sigma$) and polymer monomers in the bulk region. Then we mixed near-NP samples and bulk samples from the neat polymer system, at different ratios (5% to 50% of near-NP samples), to generate different training sets. We also construct a training set that consists only of data points from the near NP region. Using SVM as the basic classifier, we follow the protocol of TrAdaboost for 10 iterations, and take the last iterated hyperplane as the output of our training. We then use these new hyperplanes and calculate the softness profiles, the results of which are presented in Figure S15.

If the deviation in softness near the NP surface were caused by treating NP sites as polymer sites, then we would observe a positive-to-negative transition of a_i as we increase the ratio of near-NP samples. However, our measurements suggest

an inverse trend, where a_i remain positive for all the conditions measured, even for the PNC-learned plane. Varying the ratio of near-NP samples will increase or decrease softness values as a whole but does not qualitatively change our results. Thus, we believe our dynamical decomposition model is insensitive to treating NP sites as polymer sites.

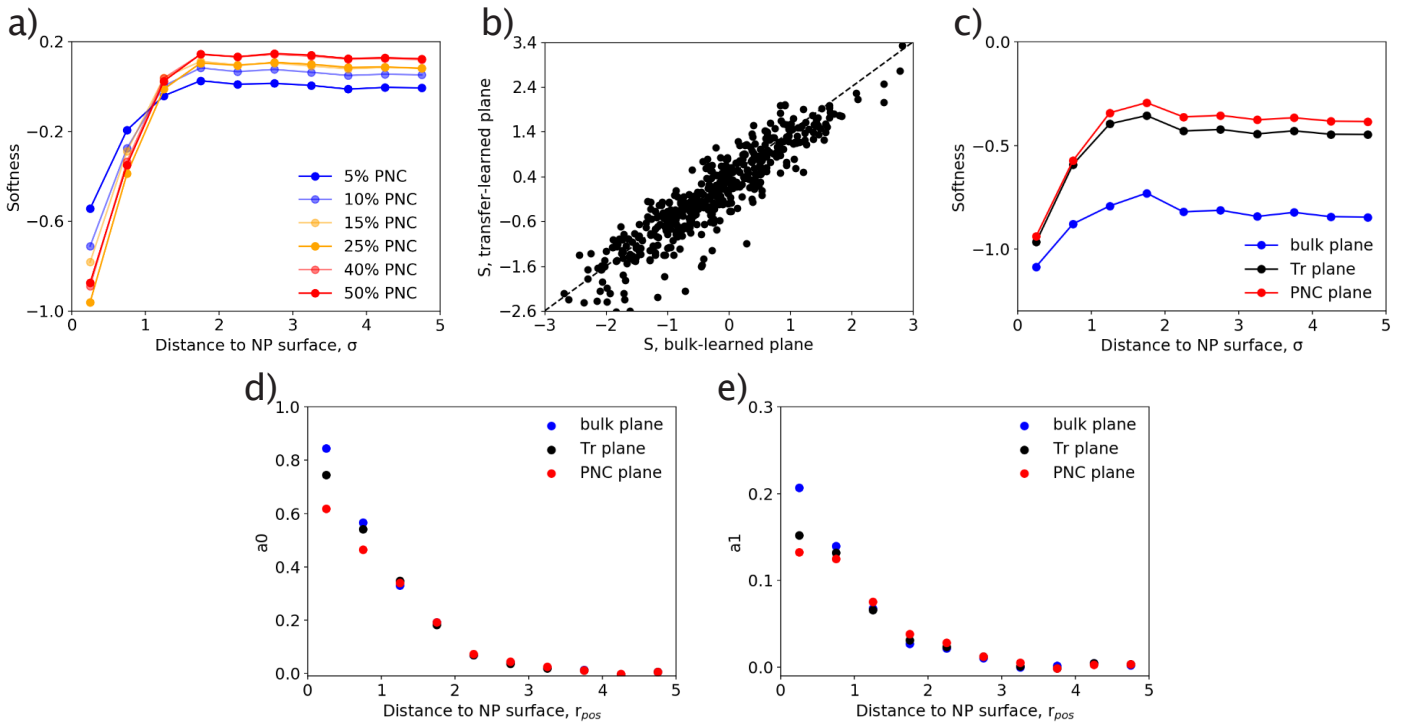

Fig. S 15 Transfer learning results in 10 *vol%* PNCs ($r_p = 3\sigma$, $\varepsilon_{pn} = 1.0$): (a) softness as a function of r_{pos} with different ratios of PNC samples, at $T = 0.40$. (b) Particle's transfer-learned softness vs. bulk-learned softness, at $T = 0.40$. Results plotted are 500 points randomly sampled from 200 frames, each frame containing 51840 polymer monomers. The dash line represents the slope of one. (c) softness as a function of r_{pos}, with bulk-learned hyperplane (blue), 10%-PNC transfer learned plane (black), and PNC-learned plane (red), at $T = 0.40$. (d) a_0 as a function of r_{pos}, at $T = 0.40$. (e) a_1 as a function of r_{pos}, at $T = 0.40$

.

Notes and references

1 S. S. Schoenholz, E. D. Cubuk, D. M. Sussman, E. Kaxiras and A. J. Liu, *Nature Physics*, 2016, **12**, 469–471.

2 E. D. Cubuk, R. J. Ivancic, S. S. Schoenholz, D. J. Strickland, A. Basu, Z. S. Davidson, J. Fontaine, J. L. Hor, Y. R. Huang, Y. Jiang, N. C. Keim, K. D. Koshigan, J. A. Lefever, T. Liu, X. G. Ma, D. J. Magagnosc, E. Morrow, C. P. Ortiz, J. M. Rieser, A. Shavit, T. Still, Y. Xu, Y. Zhang, K. N. Nordstrom, P. E. Arratia, R. W. Carpick, D. J. Durian, Z. Fakhraai, D. J. Jerolmack, D. Lee, J. Li, R. Riggleman, K. T. Turner, A. G. Yodh, D. S. Gianola and A. J. Liu, *Science*, 2017, **358**, 1033–1037.

3 E. Yang, R. J. Ivancic, E. Y. Lin and R. A. Riggleman, *Soft Matter*, 2020, **16**, 8639–8646.

4 W. Dai, Q. Yang, X. Gui-Rong and Y. Yong, *Proceedings of the 24th International Conference on Machine Learning*, 2007, 193–200.